A low-cost 3D printed microfluidic bioreactor and imaging chamber for live-organoid imaging

Ikram Khan[†*] and Anil Prabhakar
Department of Electrical Engineering, Indian Institute of Technology, Madras 600036, India.

Chloe Delepine,[†] Hayley Tsang, Vincent Pham, and Mriganka Sur
Picower Institute for Learning and Memory, Department of Brain and Cognitive Sciences, Massachusetts Institute of Technology, Cambridge, MA, 02139, USA.

(Dated: 28th March 2020)

Organoids are biological systems grown *in vitro* and are observed to self-organize into 3D cellular tissues of specific organs. Brain organoids have emerged as valuable models for the study of human brain development in health and disease. Researchers are now in need of improved culturing and imaging tools to capture the *in vitro* dynamics of development processes in the brain. Here, we describe the design of a microfluidic chip and bioreactor, to enable in-situ tracking and imaging of brain organoids on-chip. The low-cost 3D printed microfluidic bioreactor supports organoid growth and provides an optimal imaging chamber for live organoid imaging, with drug delivery support. This fully isolated design of a live-cell imaging and culturing platform enables long-term live-imaging of the intact live brain organoids as it grows. We can thus analyse their self-organization in a controlled environment with high temporal and spatial resolution.

I. INTRODUCTION

Stem cell research has revolutionized treatment developments for diseases like spinal cord injury, diabetes, rheumatoid arthritis, cerebral palsy, Alzheimer's, Parkinson's and targeted cancer treatment[1–9]. In 1907, Dr. H.V. Wilson demonstrated the potential of dissociated siliceous sponge like cells to self-organize and regenerate into a complete organism [10]. *In vitro* growth of pluripotent stem cells allows us to grow miniaturized versions of organs called organoids. Pluripotent stem cells are able to self-organize and form organoids of complex organs such as the brain, kidney, retina and heart [11–20]. Organoid based diagnosis also comes in handy for screening pharmaceutical compounds for many diseases [21–23]. Thus, organoid growth must be done in a controlled incubator environment, with careful monitoring. However, such monitoring is challenging as this involves physical handling and invasive procedures [24].

Ensuring a steady supply of nutrition to a growing organoid, continues to be one of the main issues in organoid culture. As the organoid grows bigger, its core doesn't get enough nutrient supply and gas exchange, thereby triggering cell death. Microfluidic technologies provide a solution to grow organoid in a controlled environment, and optimized perfusion of culture media. The ability to confine fluid in a small volume and being able to manipulate the cell to a higher degree of freedom has made the bio-medical research cost effective. This opened many new applications in the field of lab-on-chip [25–28]. Such small confinements are also advantageous in terms of easy integration with multiple test equipment and easier portability. Soft lithography is a common technique traditionally used for the fabrication of microfluidic devices. This is based on transferring the micro-structures from a mold to a poly-dimethylsiloxane (PDMS) [29, 30] and it also involves many other steps that limits the possible design. Recent advancement in stereo-lithography based additive manufacturing (3D printing) has made it possible to realize advanced microfluidic chips with simple manufacturing procedures [31–33]. This has dramatically brought down the cost, and the complicated steps involved in traditional manufacturing of microfluidic chips.

In this work, a low-cost microfluidic bioreactor was developed, designed to support both imaging and culture on a single chip and was fabricated using stereolithography based 3D printing. This fully standalone compact bioreactor system provides an ideal organoid culture environment with controlled temperature and media flow, avoids any chance of contamination and an imaging chamber that allows tracking of a particular cell as it grows, which was very difficult with other techniques. We believe that our work on microfluidics based 3D printed bioreactor for live-cell imaging has many advantages including low costs; a compact, mobile and standalone design; and an optimal confined environmental enclosure for 3D live organoid imaging. As the growth happens in a fully closed environment, this can be used to mimic interactions between human organoids host with pathogens like coronavirus and has potential to accelerate the development of therapeutics [34–36].

II. EXPERIMENTAL SECTION

A. Microfluidic organoid imaging platform design and fabrication

A microfluidic chip was designed as shown in Fig. 1A and Fig. 2 for the support of both imaging and culturing of organoids. Briefly, the design of the chip included imaging wells compatible with organoid long-term culture, and microfluidics channels for medium flow and pre-heating. Indi-

* Author to whom correspondence should be addressed: ikramkhan11692@gmail.com
† These authors contributed equally.

FIG. 1: (A) Imaging and organoid set-up of a well in a microfluidic chip. The design supports both organoids culturing and imaging (B) Organoid placement in the well.

vidual organoids were placed in each well of the chip, and were embedded in Matrigel, a complex extracellular environment matrix composed of natural polymers and growth factors, which acts as a scaffold for long-term growth of organoids into a 3D spheroid form. A transparent glass disk with a thickness of 150 μm was then placed on top of the well, acting both as the water seal for culture medium and as an optical window for live organoid imaging. The chip was placed on a heating plate. The culture medium providing all the required growth nutrients to the organoids was then pumped into the pre-heater chamber of the chip where it is warmed to 37 °C and distributed to one or all wells as in Fig. 2.The system was automatized using micro-controllers.

The microfluidic chip was made using stereolithography based 3D printing technology. SolidWorks (Dassault Systems) 3D CAD modeling software was used to design this chip and a ".STL" file was generated for 3D printing using a desktop 3D printer (Form 2 printer, Formlabs). A bio-compatible dental surgical grade resin (Dental SG Biocompatible Resin, Formslab) was chosen as the printing material, which supports a printing resolution of about 50 μm. The printed chip was then cured by exposure to UV light for 1 hour. The chip was sterilized with an autoclave after printing using exposure to pressurized steam at a temperature of 121°C for 30 min. The chip was designed with four culture and imaging wells. Dimensions of the wells were optimized for culture medium availability and flow, and to be compatible with the working distance of the $16\times/0.8$ NA microscope objective (Nikon) microscope objective (3mm). Small indents of 0.5 mm $\times$ 0.5 mm size were added on the inner surface of the wells, as shown in Fig. 1B, to restrict the detachment of the Matrigel from the 3D printed well. The top of the well was sealed with a glass disk of 150 μm thickness using a bio-compatible silicone (Kwik-Sil, WPI) or UV-curing (NOA61, Norland Products) adhesive. The chip thus allows examination through a transparent optical window, with excellent isolation from environmental perturbations. Each of the wells was designed with a thermistor port, and a drug delivery port, for continuous temperature logging of each well and selective drug delivery to the individual organoids, respectively. For drug delivery, a standard cannula was inserted inside the drug delivery port and sealed using a bio-compatible silicone (Kwik-Sil, WPI) or UV-curing (NOA61, Norland Products) adhesive. This cannula provides a hermetical sealing support and acts as a one-way valve for the drug delivery. The chip was designed with microfluidics channels, organized to allow media flow over the heating plate (pre-heater chamber), and then in and out the wells. One inlet for culture medium input and four outlets for each well were connected to the tubing. The system is scalable, and the number of wells can easily be increased.

The chip was connected to an incubator environment, as shown in Fig. 2, for the growth of organoids. This complete incubator and supporting devices were designed to fit into a compact form factor, with a four well chip size of 6 cm $\times$ 4 cm for easy transfer between different instruments. As the organoids take nutrition from the culture media for growth, we must periodically replace the culture media. Each well was designed to be independently selected through the use of a solenoid valve for culture media replacement. The culture media was bubbled periodically with a gas mixture of 5 % CO_2, 21 % O_2, and balanced N_2. A DC motor based small peristaltic pump (#1150, Adafruit) was used for feeding the culture media to organoids. The fluid flow was precisely controlled using a pulse width modulation (PWM) signal from the micro-controller. The details of the quantity of the culture medium and Matrigel used is shown in Table I. As the

TABLE I: Volume of Matrigel and Culture medium.

Fluid	Volume (μL)
Matrigel in 4-Wells	78$\times$ 4
Culture medium in 4-Wells	48 $\times$ 4
Volume of the culture medium in pre-heater	370

organoids require a temperature of around 37 °C for growth, a bench-top incubator environment was manufactured using aluminum blocks, where the chip is placed in close contact using screws. These aluminum blocks are black anodized to reduce the back-scattered light during imaging and to improve the thermal conductivity. A resistive heater was connected below the oven base plate and a 10 kΩ negative temperature coefficient thermistor was used for feedback to regulate the temperature of the oven. The culture media entering the chip was stored at an ambient temperature of around 25 °C, which is lower than the temperature required for the organoid growth. Such a sudden temperature change can induce a thermal shock for the organoid. To avoid this situation, an on-chip pre-heater was implemented. For uninterrupted temperature control, a dedicated micro-controller is programmed with a PID algorithm and can be controlled via USB based virtual serial port.

Fig. 3A shows the complete mechanical assembly of the microfluidic bioreactor. It has three main components: an aluminum oven, a microfluidic chip and an acrylic sheet for integration to a microscope. The oven has two parts, the first is a base heater plate that is in direct contact with the microfluidic chip, with its temperature regulated at about 37 °C. The second one is an oven cap that is used to isolate the wells from ambient temperature fluctuations. The oven cap is opened while imaging the organoids as shown in Fig. 3B and is kept closed otherwise as shown in Fig. 3C. Heat transfer through the objective lens can cause a local temperature drop at the well while imaging. Hence, the objective lens temperature should be regulated close to 37 °C using feedback driven thermal source, in long term experiments.

Our design costs are significantly lower than traditional Petri dish or spin-bioreactor based organoid culture products that can cost 10's of dollars. For 3D printing, approximately

FIG. 2: Microfluidic set-up for live cell imaging and culturing.

15 mL resin was used including the resin used for the scaffold, at a cost of only around 5 USD per chip. We also note that the culture medium used is just around 764 μL per refill.

Finally, the culture medium was pumped through each well, and the chip was ready to be combined with a pre-heated oven, shown in Fig. 4B, that kept the temperature at approximately 37 °C. Before filling the media inside the well, the chip should not be placed inside the oven. Note that we must place the chip in the oven only after filling media inside the well. This ensures that the water content in the Matrigel does not evaporate and condense on the glass surface, trapping air, and affecting the quality of the optical image.

After the imaging experiments, the silicone glue used to seal the glass coverslip on top of each well can be easily removed and the organoids collected for post hoc assays such as IHC, RNA/DNA/protein extraction and quantification. After removal of the glass coverslips, the organoids, and the Matrigel, a chip can be washed with distilled water, dried, and autoclaved; and is therefore re-usable.

Fig. 4C shows the complete system developed for an organoid culture in an incubation environment.

B. Production of cerebral organoids

Brain organoids were produced from iPSC obtained from the Coriell cell line repository (GM23279A) following a standard protocol (Mellios et al. 2018) . iPSC colonies were grown in iPSC media, consisting of 20% Knockout Serum Replacement (KOSR) (Invitrogen), 1% penicillin/streptomycin (Invitrogen), 1% non-essential amino acids (Invitrogen), 0.5% L-glutamine (Invitrogen), 100 μm 2-mercaptoethanol (Bio-Rad), DMEM/F-12 (Invitrogen), supplemented with 10 ng/mL bFGF (Stemgent). The culture media was changed daily. iPSC colonies were passaged weekly onto 6-well plates coated with 0.1% gelatin (EMD Millipore) and pre-seeded with a feeder layer of irradiated mouse embryonic fibroblasts (MEFs) (GlobalStem), which were plated at a density of 200,000 cells/ well. Passaging entailed lifting colonies with 2.5 mg/ml Collagenase, Type IV (ThermoFisher) for 1 hr and dissociation into smaller pieces through manual tritulation before seeding onto feeder layer of MEFs. iPSCs were detached from irradiated MEFs and plated at 9×10^4 cells per well of an ultra-low attachment 96-well plate (Corning) in iPSC media supplemented with bFGF (10 ng/mL) and ROCK inhibitor (50 μm; Y-27632, Tocris) (Day 0). Embryoid bodies (EBs) were subsequently transferred (Day 6) to an ultra-low attachment 24-well plate (Corning) with neural induction media: 1% N_2 supplement (Invitrogen), 1% Glutamax (Invitrogen), 1% non-essential amino acids (Invitrogen), 5 ug/mL heparin (Sigma), DMEM/F12 (Invitrogen), supplemented with 10 μm SB431542 (Tocris Bioscience) and 1 μm dorsomorphin (Stemgent). After this neural induction step, EBs were embedded in Matrigel (Corning) droplets on Day 11 and transferred to neural differentiation media: DMEM/F12: Neurobasal (Invitrogen), 0.5% N_2 supplement, 1% Glutamax, 0.5% non-essential amino acids, 100 μm 2-mercaptoethanol, insulin, 1% Pen/Strep (Invitrogen) supplemented with 1% B27 without vitamin A (Gibco, Life Technologies). Matrigel embedded organoids can then be placed in the chip from D11 onward. For the fluorescence imaging of radial glial cells, organoids were infected with a pAV-CMV-GFP virus prior to embedding in the chip.

FIG. 3: Microfluidic bioreactor assembly (A) Exploded view of bioreactor (B) Imaging mode (C) Incubation mode.

C. Organoids deployment in microfluidic chip

Initially, Matrigel of around 45 μL was filled inside each well and let to solidify for 20 minutes at room temperature. Then, organoids at day 15 of differentiation were selected and placed in the center of each well, and another layer of Matrigel was applied on top of the organoids, letting them solidify at room temperature. This sandwiching process gave an extracellular scaffold for organoids to grow as a 3D spheroid. The scaffold also held organoids inside the well against the current of culture medium. Finally, a 12 mm microscope glass disk was kept on the top of the well and was sealed with silicone or UV-curing adhesive. Fig. 4A shows the full set up of the microfluidic chip containing organoids positioned inside the wells, culture medium flow, and the thermistor probe.

D. Cryosectioning and immunohistochemistry

For the analysis of viability, organoids were fixed by a 30 min incubation in 4% paraformaldehyde solution. Fixed organoids were incubated in 20% sucrose solution overnight at 4 °C, followed by incubation in 30% sucrose for 3 hours before embedding and freezing in optimal cutting temperature (O.C.T) medium. Frozen organoid tissue was sliced into 20 μm sections using a cryostat. Permeabilization/blocking was performed using 3% BSA/ 0.1% TX100 in TBS. Incubation of sections from cerebral organoids in primary antibodies solution was performed overnight at 4 °C and in secondary antibodies solution at room temperature for 1 hour (Alexa Fluor, Molecular Probes). The following primary antibodies were used: cleaved caspase 3 (Cell Signaling, #9661, 1:200), Ki67 (BD Biosciences, #550609, 1:200). Coverslips were affixed

FIG. 4: Microfluidic bioreactor. (A) Organoids deployment in microfluidic chip (B) Bioreactor integration with control system (C) Compact standalone bioreactor.

with vectashield hardset antifade mounting media with DAPI (Vector Laboratories) and z-stacks were acquired using a Leica TCS SP8 confocal microscope.

E. Two-photon microscopy

The imaging was performed using a Prairie Ultima IV two-photon microscopy system with a galvo-galvo scanning module (Bruker). A 910 nm wavelength excitation light was provided by a tunable Ti:Sapphire laser (Mai-Tai eHP, Spectra-Physics) with dispersion compensation (DeepSee, Spectra-Physics). For collection, we used a $16\times/0.8$ NA microscope objective (Nikon) and a GaAsP photomultiplier tubes (Hamamatsu), that allowed us to image a large number of cells. Images thus acquired, using a PrairieView acquisition software, were then processed using the ImageJ software.

III. RESULTS AND DISCUSSION

A. Experimental and simulation results of the oven

For the heater, a 20 Ω, TO-126 package resistor was used with a 10 kΩ negative resistance coefficient (NTC) thermistor for feedback, as shown in Fig. 5A. A PID control algorithm, running on an Atmega328p microcontroller with a LM298 H-bridge driver, was used for controlling the current through the heater. The controller measures the temperature of the oven and compares it with the target temperature of 37 °C and computes the error signal $e(t)$. Based on the error response signal, $u(t)$ is calculated with proportional (P), integral (I) and derivative (D) terms as,

$$u(t) = K_p e(t) + K_i \int_0^t e(t')dt' + K_d \frac{de(t)}{dt} \qquad (1)$$

FIG. 5: Oven temperature controller (A) 3D model (B) Temperature controller block diagram.

The magnitude of $u(t)$ is mapped to the duty cycle of the PWM signal pin, as shown in Fig. 5B. Based on the value of $u(t)$, the duty cycle will be adjusted such that error reaches zero. The P block is a gain factor to amplify the error, I block is for calculating cumulative error, integrated over time, to eliminate the residual error, and the D block gives the rate of error change (more rapid the error change, greater the damping effect). The K_p, K_i, and K_d constants were optimized in the program for precise temperature control with fast settling, integrated over 13 minutes. A thermally conductive paste was applied between the heater and the oven for efficient thermal control. It is important to replace this paste after using for a few months for ensuring good thermal conductivity.

The thermal simulation was carried out in SolidWorks to study the thermal gradient along the organoids in the wells. Fig. 6A shows the steady state result of the microfluidic chip with organoids modelled as a spherical mass, with a mass density 1050 kg/m^3, thermal conductivity of 0.53 W/(m.K) and a specific heat 3690 J/(kg.K). Their corresponding thermal gradient is shown in Fig. 6B. We observed that the temperature was successfully maintained around 37 °C, with the maximum temperature difference across the four well being less than 0.21 °C at steady state.

FIG. 6: Oven thermal simulation (A) Temperature distribution on chip (B) Temperature distribution less than 0.21 °C across all the wells.

A PID temperature controller was connected to the oven heater and to the feedback thermistor. The experimental temperature inside the four wells was measured, as shown in Fig. 7A. We notice that the oven reached a steady state after about 12 minutes. The box-and-whisker plot computed for the data at steady state temperature is shown as an inset in Fig. 7A. This steady state temperature data was acquired for around 12 hours, and from the box plot, it can be observed that the median was around 37.6 °C and 50 % of the data was 0.2 °C around the mean. The maxima and minima shown by the whiskers are within 0.4 °C. The steady state data temperature tolerance is shown in Fig. 7B. We note that the oven was regulating the temperature within ± 0.5 % tolerance around 37.4 °C.

FIG. 7: Oven experimental results. (A) Real-time temperature data from oven (B) Temperature tolerance histogram over the set temperature of 37.4 °C.

B. Culture medium flow control and pre-heater

The culture medium, containing 191 μL inside the wells, was replaced within 6 seconds by using a calibrated flow rate of around 33.75 μL/s. Such precise calibration was achieved by using a PWM based control with a change in duty cycle translating to the speed of the peristaltic pump. The Reynolds number for this microfluidic channel of 2 mm $\times$ 0.5 mm and 33 μL/s flow rate was around 263, indicating a laminar flow inside the channel. The culture medium needs to be pre-heated to avoid any thermal shock to the organoids. Fig. 8 shows the simulation results of the on-chip pre-heater. The culture media at an ambient temperature of 25 °C is passed through the coils of the microfluidic channels, and the temperature is regulated to 37 °C using a resistive heater. The fluid delivered to the wells was thus optimized to be close to 37 °C (35.49 °C to 36.61 °C).

FIG. 8: Pre-heater flow optimization.

C. Viability

To assess the viability of organoids grown in the stage-top microfluidic bioreactor, we measured the percentage of cells expressing the proliferation marker Ki67 and apoptotic marker cleaved caspase 3 (c-Cas3). We examined the ventricular zones (VZ), structures organized around a cavity or ventricle that resemble the developing neocortex, and the core region of organoids grown for 7 days in the bioreactor or grown in a regular culture environment. We observed no significance difference in the percentage of proliferative cells (Fig. 9). Moreover the percentage of apoptotic cells in both the ventricular zone and the organoid core were decreased in organoids cultured in the microfluidic bioreactor compared to regular culture conditions supporting good viability of the organoid grown in the bioreactor. One advantage offered by our microfluidic device is that it allows continuous perfusion of the culture chamber, which more closely mimics a physiological tissue perfusion, than conventional culture, and thus reduces cell death at the organoid core.

FIG. 9: (A) Representative images of immuno-labeling of proliferation marker Ki67 and apoptosis marker cleaved caspase 3 (c-Cas3). Scale bar represents 200 μm.(B) Quantification of the percentage of positive cells.

D. Chronic imaging of brain organoid growth

Our stage-top incubator with automated fluidic-system containing embedded organoids was placed under a two-photon microscope, that allowed us to capture images despite the challenges of high density and opacity of the organoids. We performed chronic imaging, and obtained high resolution imaging of intact organoids from the surface to a depth of 100 - 200 μm, capturing either intrinsic (autofluorecence, second harmonic generation) or fluorophore (GFP expression) signals. First, we successfully imaged the growth of organoids embedded in the chip during 7 days as shown in Fig. 10. We observed an increase in volume of the 3D structure (1.88-fold after 7 days), supporting the high viability of the organoids and suggesting the organoid can expand through normal cell division growth in the bioreactor.

FIG. 10: (A) Carton figure (up, left) and 3D rendering of the intrinsic originated from the surface (856 x 856 x 240 μm) of an organoid growing in the microfluidic stage-top bioincubator . Scale bar represents 200 μm.(B) Quantification of relative growth.

E. High resolution time-lapse imaging and cell tracking

Brain organoids contain ventricular zones (VZ) (Fig. 11A). These regions contain several brain cell types, including neurons, and radial glial cell that expand their processes radially to guide neuronal migration (Fig. 11A). We were able to image the intrinsic signal emitted in these regions, demonstrating the use of the microfluidic bioreactor for applications such as 3D and time lapse imaging of organoid VZs, as shown in Fig. 11. Such imaging can be used for the tracking of single cells and the analysis of their displacement.

Finally, we expressed a GFP construct selectively in radial glial cells, which allow us to image with extremely high resolution the morphology and organization of these polarized cells after organoids were embedded and cultured in the microfluidic bioreactor as shown in Fig. 12A. We performed time lapse imaging and observed changes in cell morphology as shown in Fig. 12B.

IV. CONCLUSION

A 3D organoid in-vitro culture microfluidic device was designed and fabricated to allow chronic imaging of the dynamics involved in organoid self-assembly. Traditionally, organoids were grown in a Petri dish, which was not very efficient and required a large volume of culture media. Improved long-term culture came from bioreactors like rotary cell culture system (RCCS), Spin Omega (SpinΩ), and Spin Infinity (Spin∞), that have shown significant improvement for long-term organoid growth [37–42]. However, these bioreactors do not support a means for examination/imaging without a physical transfer of the organoids to a separate imaging chamber [43]. The transfer process is prone to organoid damage or contamination, which can lead to inaccurate estimation and limited reproducibility of the results. Hence, we needed a system equipped with the capacity to permit long-term imaging and

FIG. 11: Imaging of the second harmonic signal from brain organoids ventricular zones (VZ). (A) Cartoon figure of the VZ structures contained in a cortical organoid. (B) 3D reconstruction and 2D z sections of an organoid. The field of view contained several VZ structures. Yellow square indicate the field-of-view magnified in C. (C) Magnified time lapse imaging of one VZ structure demonstrated that global cell movement can be tracked. (D) Left image is a time colored projection of the timelapse imaging. The VZ area is deliminated with yellow dashed lines. Example individual cells are indicated with colored arrows. Scale bars represent 200 μm.

FIG. 12: High resolution two-photon microscopy imaging of GFP-labelled radial glial cells in a brain organoid embedded and cultured in the microfluidic chip and bioreactor. (A) Example images of dense populations of GFP positive radial glial cells organized radially around a ventricle-like cavity. The fine morphology of individual cells can be distinguished. Scale bar represents 100 μm (B) Example of high magnification time lapse imaging revealing changes in cell morphology. Left image is a time colored projection of the timelapse imaging. Scale bar represents 20 μm.

limited disturbance of organoids grown in an incubator like environment.

Current practices for brain organoid live imaging typically use commercial culture dishes such as a 96-well glass-bottom plate (Corning #4580). These plates are costly, do not provide an optimized compartment for organoid growth, and do not allow for media change/perfusion during imaging [44, 45]. Some researchers have used commercial culture dishes, combined with microfabricated compartments. These again involve complicated fabrication of PDMS stamps using a metal mold [46]. They also typically require the use of an inverted confocal microscope that is associated with an environmentally controlled chamber [44–48]. The use of a conventional incubation system for culture, separated and different from the environmentally controlled chamber for imaging, induces a variation in the culture environment and can lead to cellular stress. In recent years, many microfluidic organoids-on-a-chip systems have been developed, demonstrating that this culture model is useful. These organoid-on-a-chip systems continue to improve, and are becoming useful in organ and disease modeling, and drug discovery studies [26, 49, 50]. However, most organoid-on-a-chip platforms are limited by the use soft lithography, a technically demanding microfabrication process. Our system has the advantage of being easily manufactured, via 3D printing, and is more versatile than the aforementioned systems published in the literature. In our design, chip printing is cheap and easily adjustable. It is adaptable to any microscope, including non-standard custom made or upright microscopes. Moreover, our design provides a fully enclosed system, allowing for a sterile and safe working condition, with continuous perfusion of a nutrient-rich culture medium. We also have precise control of the cell environment and can keep it invariant during both the growth and imaging steps of organoid cultures.

The 3D printed microfluidic chip with imaging chambers and drug delivery system functions with a temperature controller and a pump to create an isolated and compact bioreactor that can be installed temporally into a microscope for live imaging. We demonstrated the use of this bioreactor for imaging of a brain organoid expansion and cell morphology tracking for up to 7 days. As we observed normal organoid growth during this long-term incubation, we expect than the organoid could grow for extended periods of time with the only constrain of the dimension of the wells. Our 3D printed microfluidic bioreactor for the culture and live-imaging of 3D biological tissues can find its applications in many research or industrial laboratories where organoids can be modeled to study development, diseases, or interactions between human host organoids and pathogens like coronavirus SARS-COV2. It is a low cost solution compared to traditional laboratory methods, with a fabrication price of around 5 USD per chip, and an efficient microfluidic delivery of the expansive culture media.

Onging work includes the scaling up the number of wells and integration of additional features like electrophysiology to study the organoid model. In future, the microfluidic valves and pumps can also be 3D printed on-chip to reduce the amount of culture medium used.

AVAILABILITY OF THE DATA

The data that support the findings of this study are available from the corresponding author upon reasonable request.

ACKNOWLEDGEMENTS

This work was supported by National Institutes of Health (NIH) grant R01MH085802 (M.Sur) and the Centre for Computational Brain Research, IIT Madras. M.Sur holds the N.R. Narayanamurthy Visiting Chair Professorship in Computational Brain Research at IIT Madras. I. Khan was supported by the Dept. of Biotechnology vide grant BIRAC-BT/BIPP0946/36/15, and C. Delepine by the Picower Fellowship Program. We also thank members of the Sur lab and the Photonics Group, Electrical Engg., IIT Madras for their support.

[1] N. Nagoshi, O. Tsuji, M. Nakamura, and H. Okano, Regenerative Therapy **11**, 75 (2019).
[2] X. Hu, X. Zhou, Y. Li, W. Tang, and Q. Chen, International Journal of Developmental Neuroscience **76**, 80 (2019).
[3] S. Mostafa, R. Jafarzadeh-esfehani, S. Mahdi, S. Mohammad, R. Parizadeh, S. Vojdani, and M. Ghandehari, International Journal of Biochemistry and Cell Biology **110**, 75 (2019).
[4] D. Ma, K. Xu, G. Zhang, Y. Liu, J. Gao, M. Tian, C. Wei, J. Li, and L. Zhang, International Immunopharmacology **74**, 105687 (2019).
[5] L. Zhang and J. Zhang, Life Sciences **246**, 117405 (2020).
[6] A. A. Stock, V. Manzoli, T. D. Toni, M. M. Abreu, Y. Poh, L. Ye, A. Roose, F. W. Pagliuca, C. Thanos, C. Ricordi, and A. A. Tomei, Stem Cell Reports **14**, 91 (2020).
[7] J. B. Sneddon, Q. Tang, P. Stock, J. A. Bluestone, S. Roy, and T. Desai, Cell Press **22**, 810 (2018).
[8] X. Xia, J. He, and R. Aji, Cancer Letters **457**, 20 (2019).
[9] N. H. A. Chahine, T. W. Wehbe, R. A. Hilal, V. V. Zoghbi, A. E. Melki, and E. B. B. Habib, International Journal of Stem Cells **9**, 90 (2016).
[10] H. V. Wilson, Science **25**, 912 (1907).
[11] A. Taguchi, Y. Kaku, T. Ohmori, S. Sharmin, M. Ogawa, H. Sasaki, and R. Nishinakamura, Cell Stem Cell **14**, 53 (2014).
[12] Y. Xia, E. Nivet, I. Sancho-Martinez, T. Gallegos, K. Suzuki, D. Okamura, M. Z. Wu, I. Dubova, C. R. Esteban, N. Montserrat, J. M. Campistol, and J. C. Izpisua Belmonte, Nature Cell Biology **15**, 1507 (2013).
[13] H. Wu, K. Uchimura, E. L. Donnelly, Y. Kirita, S. A. Morris, and B. D. Humphreys, Cell Stem Cell **23**, 869 (2018).
[14] M. A. Mostajo-Radji, M. T. Schmitz, S. T. Montoya, and A. A. Pollen, Brain Research **1729**, 146582 (2020).
[15] M. J. Brooks, H. Y. Chen, R. A. Kelley, A. K. Mondal, K. Nagashima, N. De Val, T. Li, V. Chaitankar, and A. Swaroop, Stem Cell Reports **13**, 891 (2019).
[16] B. Nugraha, M. F. Buono, and M. Y. Emmert, European Heart Journal **39**, 4234 (2018).
[17] M. A. Lancaster and J. A. Knoblich, Science **345**, 6194 (2014).
[18] K. Takahashi and S. Yamanaka, Cell **126**, 663 (2006).
[19] K. Takahashi, K. Tanabe, M. Ohnuki, M. Narita, T. Ichisaka, and K. Tomoda, Cell **131**, 861 (2007).
[20] K. Okita, T. Ichisaka, and S. Yamanaka, Nature Articles **448**, 313 (2007).
[21] M. S. Elitt, L. Barbar, and P. J. Tesar, Human molecular Genetics **27**, 89 (2018).
[22] A. Farkhondeh, R. Li, K. Gorshkov, K. G. Chen, M. Might, S. Rodems, D. C. Lo, and W. Zheng, Drug Discovery Today **24**, 992 (2019).
[23] J. Kondo and M. Inoue, Cells **8**, 470 (2019).
[24] G. Kim, N. J. Ginga, and S. Takayama, Cellular and Molecular Gastroenterology and Hepatology **6**, 123 (2018).
[25] D. H. Sunghee Estelle Park, Andrei Georgescu, Organoids **965**, 960 (2019).
[26] A. Skardal, T. Shupe, and A. Atala, Drug Discovery Today **21**, 1399 (2016).
[27] J. Aleman and A. Skardal, Biotechnology and Bioengineering **116**, 936 (2019).
[28] A. Lin, F. Sved Skottvoll, S. Rayner, S. Pedersen-Bjergaard, G. Sullivan, S. Krauss, S. Ray Wilson, and S. Harrison, Electrophoresis **41**, 56 (2020).
[29] S. Torino, B. Corrado, M. Iodice, and G. Coppola, Inventions **3**, 1 (2018).
[30] H. M. Wu, T. A. Lee, P. L. Ko, H. J. Chiang, C. C. Peng, and Y. C. Tung, Journal of Micromechanics and Microengineering **28**, 043001 (2018).
[31] A. K. Au, W. Huynh, L. F. Horowitz, and A. Folch, Angewandte Chemie - International Edition **55**, 3862 (2016).
[32] S. J. Leigh, H. T. Gilbert, I. A. Barker, J. M. Becker, S. M. Richardson, J. A. Hoyland, J. A. Covington, and A. P. Dove, Biomacromolecules **14**, 186 (2013).
[33] O. Moreno-Rivas, D. Hernández-Velázquez, V. Piazza, and S. Marquez, Materials Today: Proceedings **13**, 436 (2019).
[34] M. A. Duque-Correa, R. M. Maizels, R. K. Grencis, and M. Berriman, Trends in Parasitology **36**, 170 (2020).
[35] J. Barrila, A. Crabbé, J. Yang, K. Franco, S. D. Nydam, R. J. Forsyth, R. R. Davis, S. Gangaraju, C. Mark Ott, C. B. Coyne, M. J. Bissell, and C. A. Nickerson, Infection and Immunity **86**, 1 (2018).
[36] I. Dickson, Nature Reviews Gastroenterology & Hepatology **17**, 383 (2020).
[37] M. A. Phelan, P. I. Lelkes, and A. Swaroop, Stem Cell Investigation **13**, 565 (2018).
[38] X. Lei, L. Ning, Y. Cao, S. Liu, S. Zhang, and Z. Qiu, Plos One **6**, 1 (2011).
[39] G. Cossellu, A. Ottonello, D. Kaigler, and G. Mazzoleni, Tissue Engineering **24**, 187 (2017).
[40] T. DiStefano, H. Y. Chen, C. Panebianco, K. D. Kaya, M. J. Brooks, L. Gieser, N. Y. Morgan, T. Pohida, and A. Swaroop, Stem Cell Reports **10**, 300 (2018).
[41] X. Qian, H. N. Nguyen, M. M. Song, C. Hadiono, S. C. Ogden, C. Hammack, B. Yao, G. R. Hamersky, F. Jacob, C. Zhong, K. J. Yoon, W. Jeang, L. Lin, Y. Li, J. Thakor, D. A. Berg, C. Zhang, E. Kang, M. Chickering, D. Nauen, C. Y. Ho, Z. Wen, K. M. Christian, P. Y. Shi, B. J. Maher, H. Wu, P. Jin, H. Tang, H. Song, and G. L. Ming, Cell **165**, 1238 (2016).
[42] X. Qian, F. Jacob, M. M. Song, H. N. Nguyen, H. Song, and G. L. Ming, Nature Protocols **13**, 565 (2018).
[43] S. A. Sloan, S. Darmanis, N. Huber, T. Khan, F. Birey, C. Caneda, R. Reimer, S. R. Quake, B. A. Barres, and P. Sergiu, Neuron **95**, 779 (2018).
[44] F. Birey, J. Andersen, C. D. Makinson, S. Islam, W. Wei, N. Huber, H. C. Fan, K. R. C. Metzler, G. Panagiotakos, N. Thom, N. A. Oâ^{TM}Rourke, L. M. Steinmetz, J. A. Bernstein, J. Hallmayer, J. R. Huguenard, and S. P. PaÅŸca, Nature **545**, 54 (2017).
[45] Y. Miura, M.-Y. Li, F. Birey, K. Ikeda, O. Revah, M. V. Thete, J.-Y. Park, A. Puno, S. H. Lee, M. H. Porteus, and S. P. PaÈ^{TM}ca, Nature Biotechnology **38**, 1421 (2020).
[46] E. Karzbrun, R. Y. Tshuva, and O. Reiner, Current Protocols in Cell Biology **81**, 1 (2018).
[47] J. A. Bagley, D. Reumann, S. Bian, J. LÃ©vi-Strauss, and J. A. Knoblich, Nature Methods **14**, 743 (2017).
[48] J. Klaus, S. Kanton, C. Kyrousi, A. C. Ayo-Martin, R. Di Giaimo, S. Riesenberg, A. C. Oâ^{TM}Neill, J. G. Camp, C. Tocco, M. Santel, E. Rusha, M. Drukker, M. Schroeder, M. GÃ¶tz, S. P. Robertson, B. Treutlein, and S. Cappello, Nature Medicine **25**, 561 (2019).
[49] F. Yu, W. Hunziker, and D. Choudhury, Micromachines **10** (2019), 10.3390/mi10030165.
[50] F. Duzagac, G. Saorin, L. Memeo, V. Canzonieri, and F. Rizzolio, Cancers **13** (2021), 10.3390/cancers13040737.

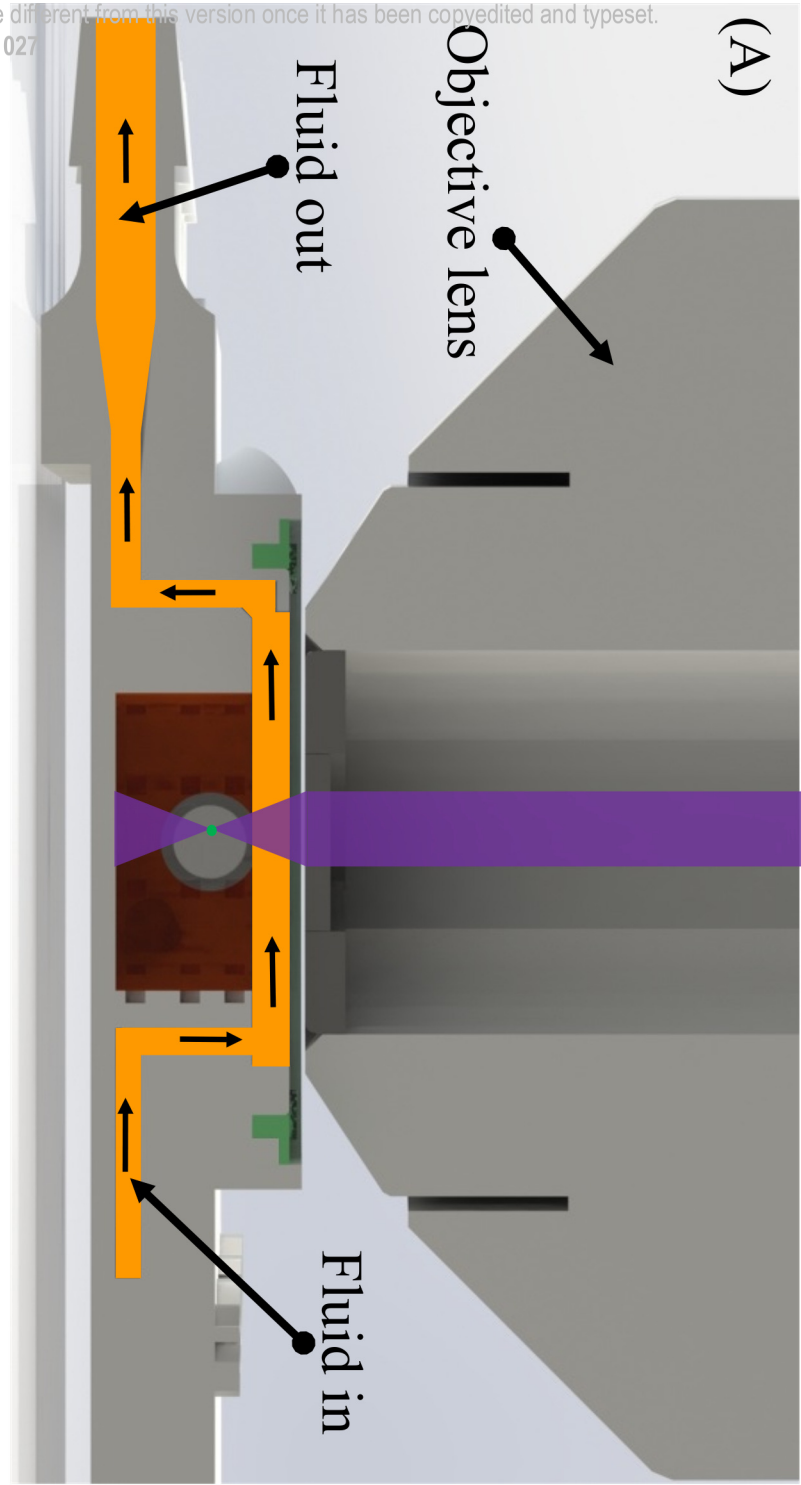

PLEASE CITE THIS ARTICLE AS DOI: 10.1063/5.0041027

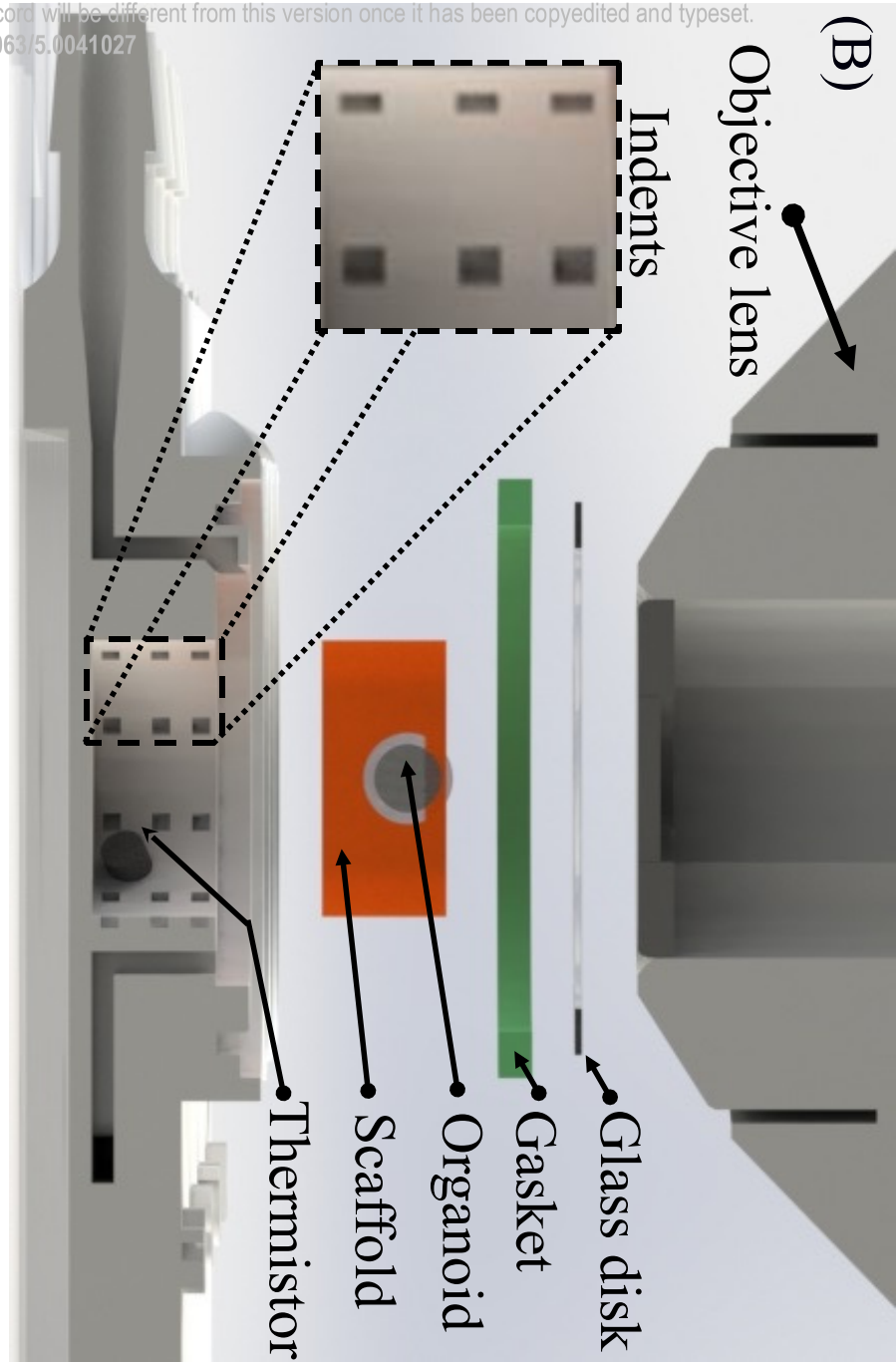

Biomicrofluidics

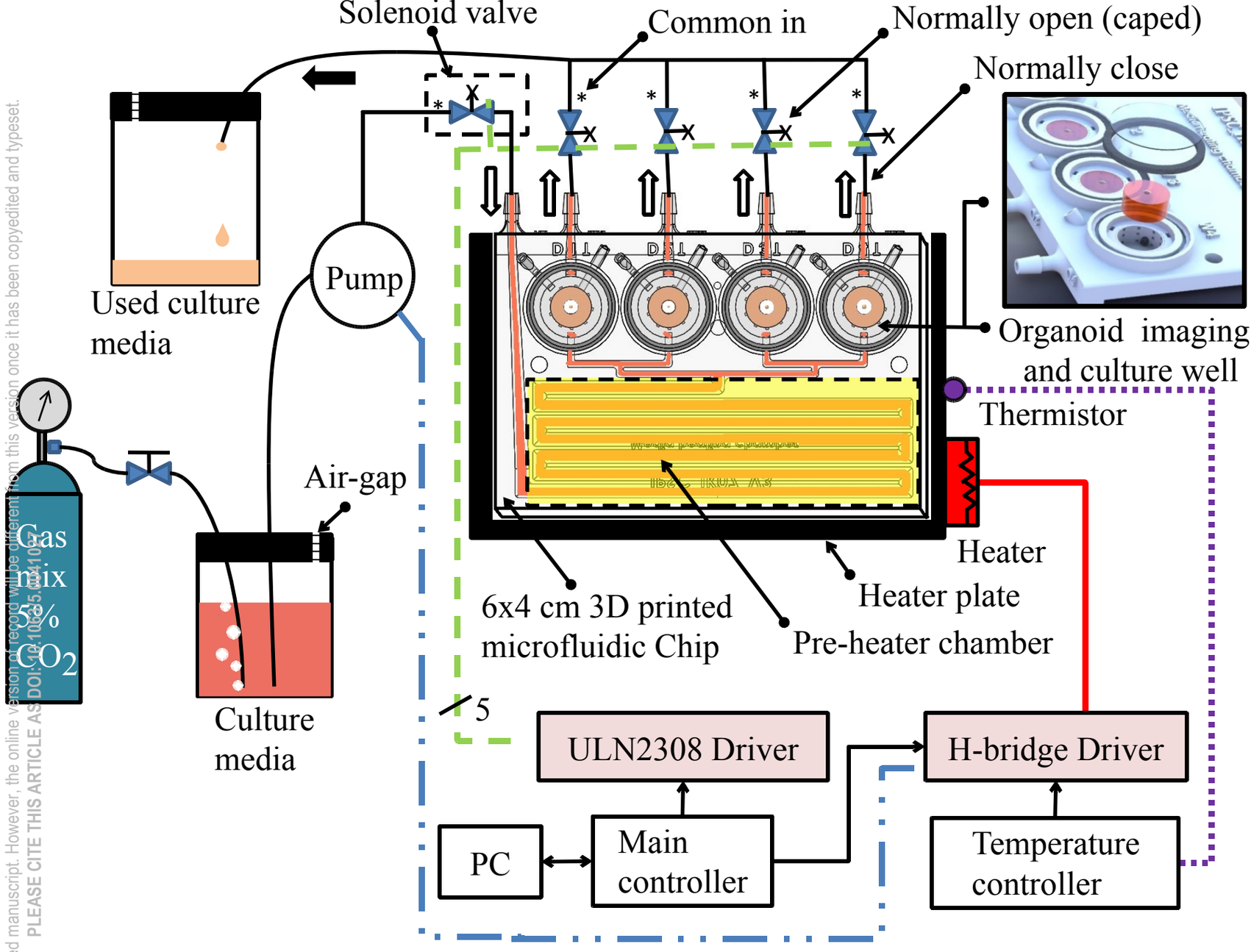

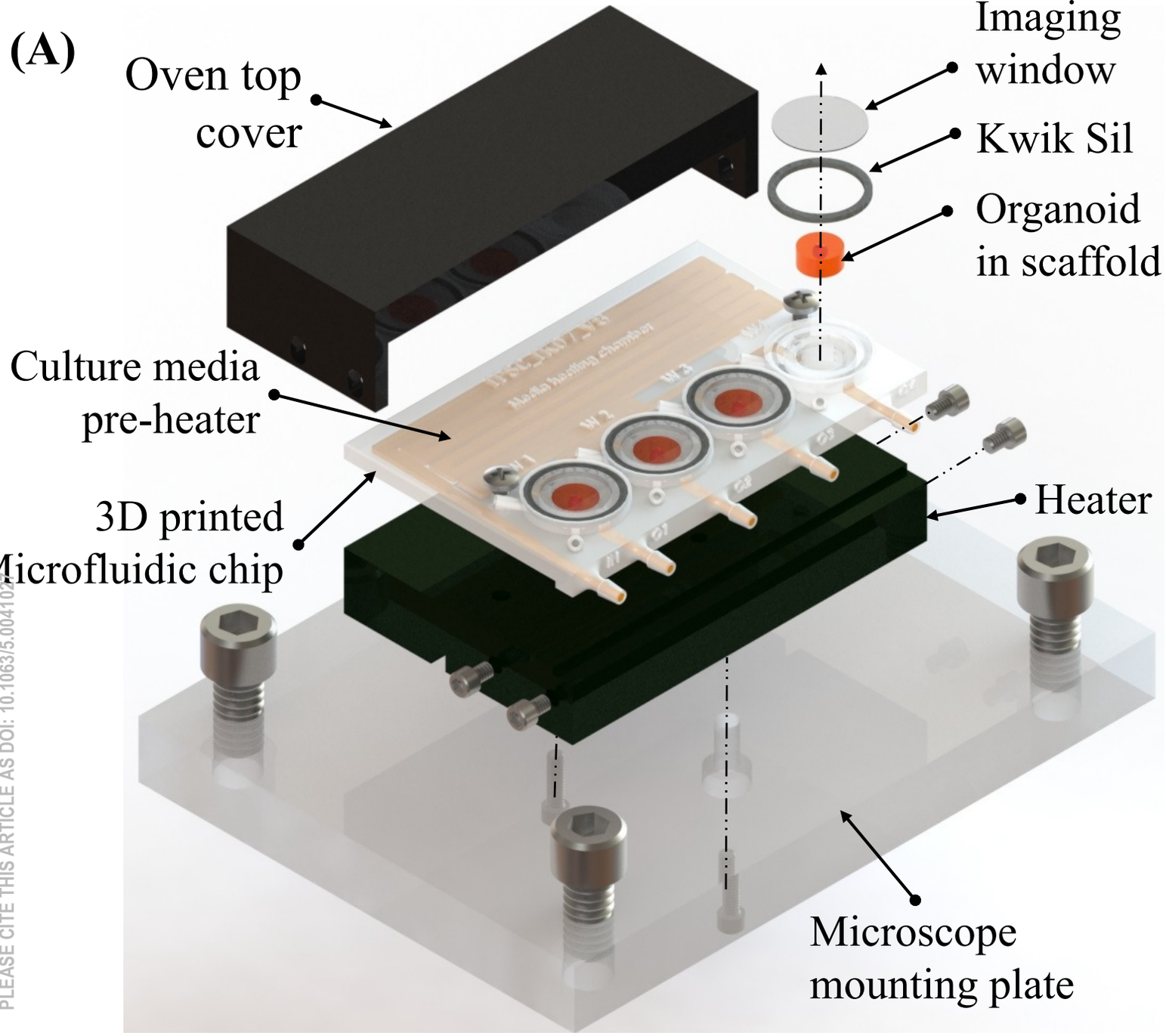

AIP Publishing

Biomicrofluidics

ACCEPTED MANUSCRIPT

PLEASE CITE THIS ARTICLE AS DOI: 10.1063/5.0041027

(B)

Biomicrofluidics

PLEASE CITE THIS ARTICLE AS DOI: 10.1063/5.0041027

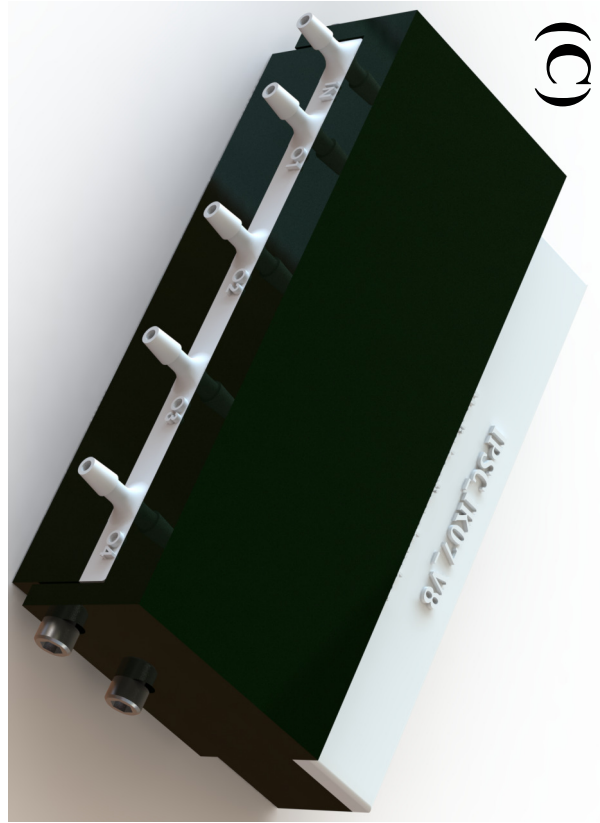

Biomicrofluidics

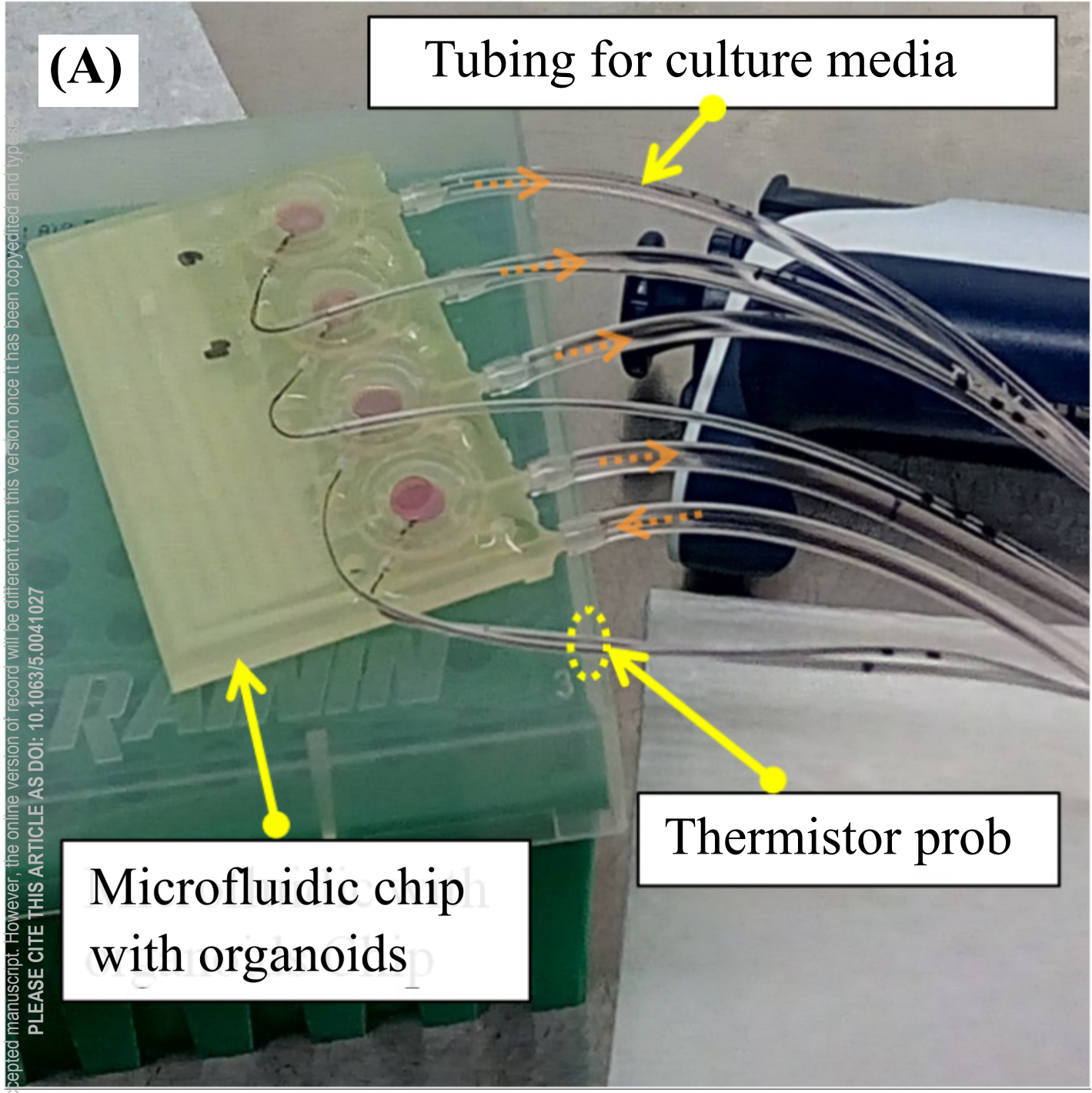

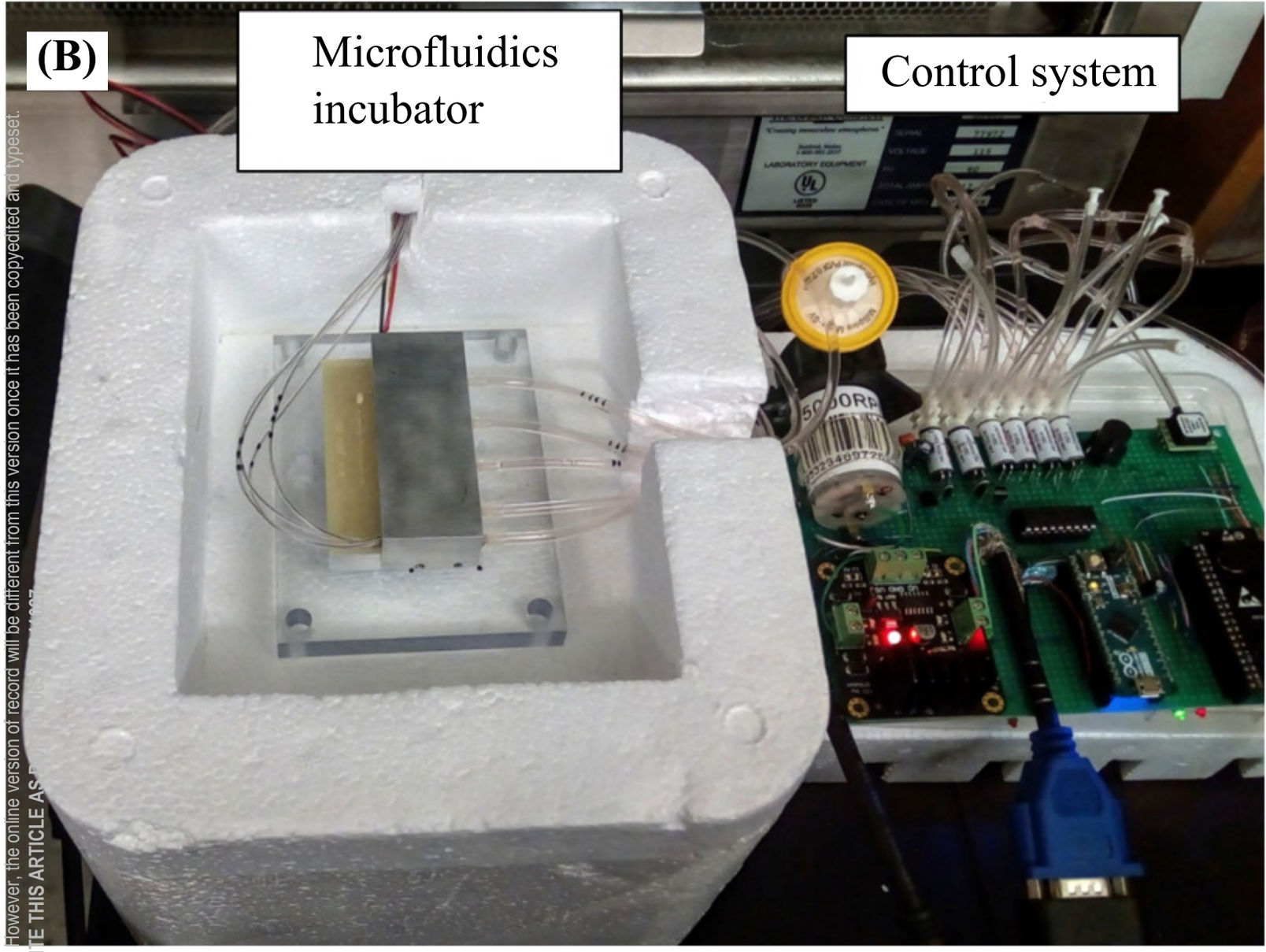

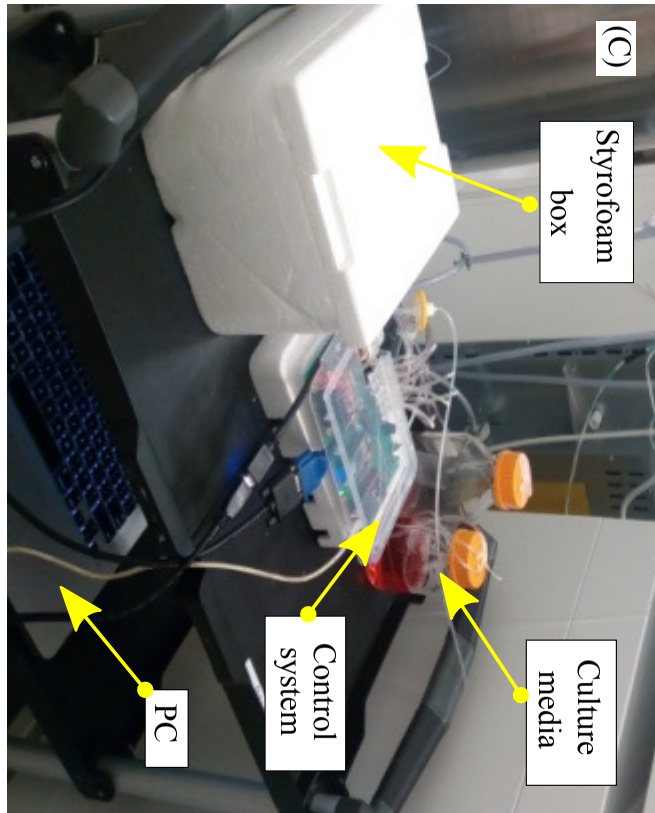

(A)

(B)

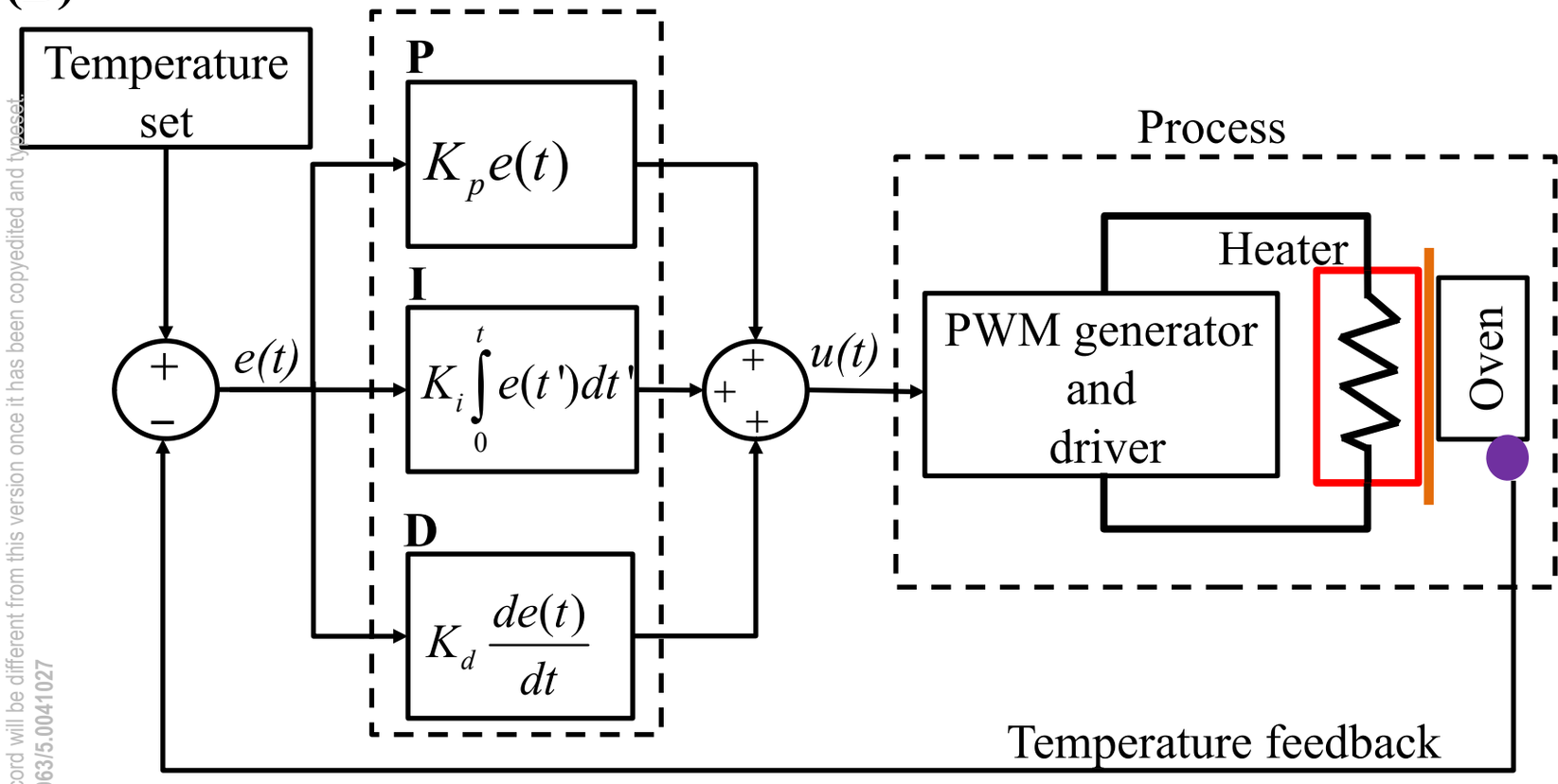

(A)

(B)

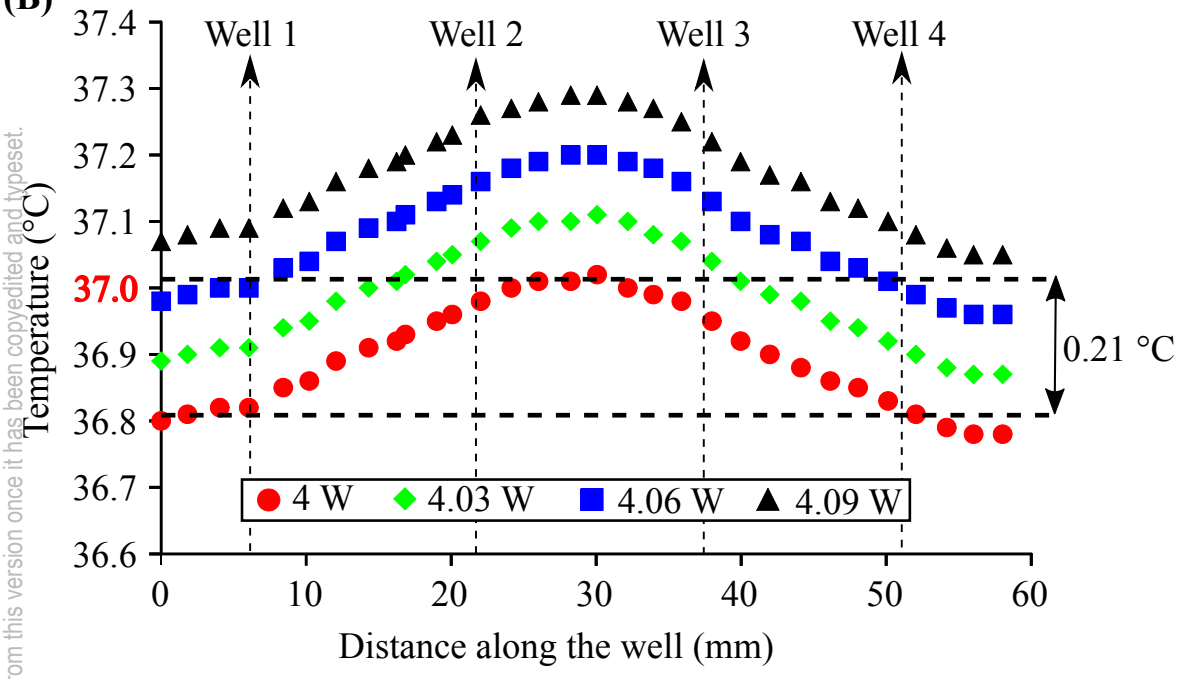

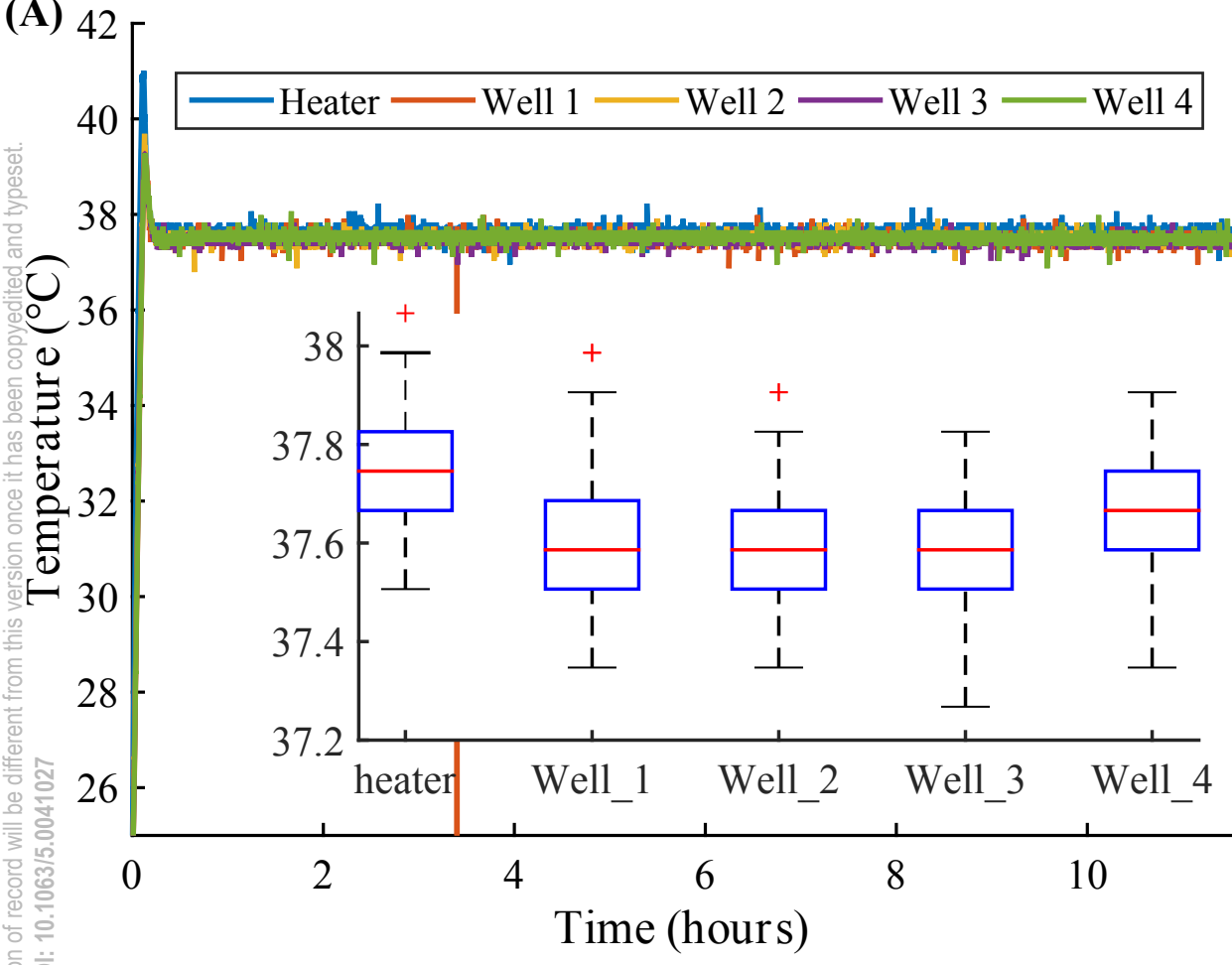

(B)

PLEASE CITE THIS ARTICLE AS DOI: 10.1063/5.0041027

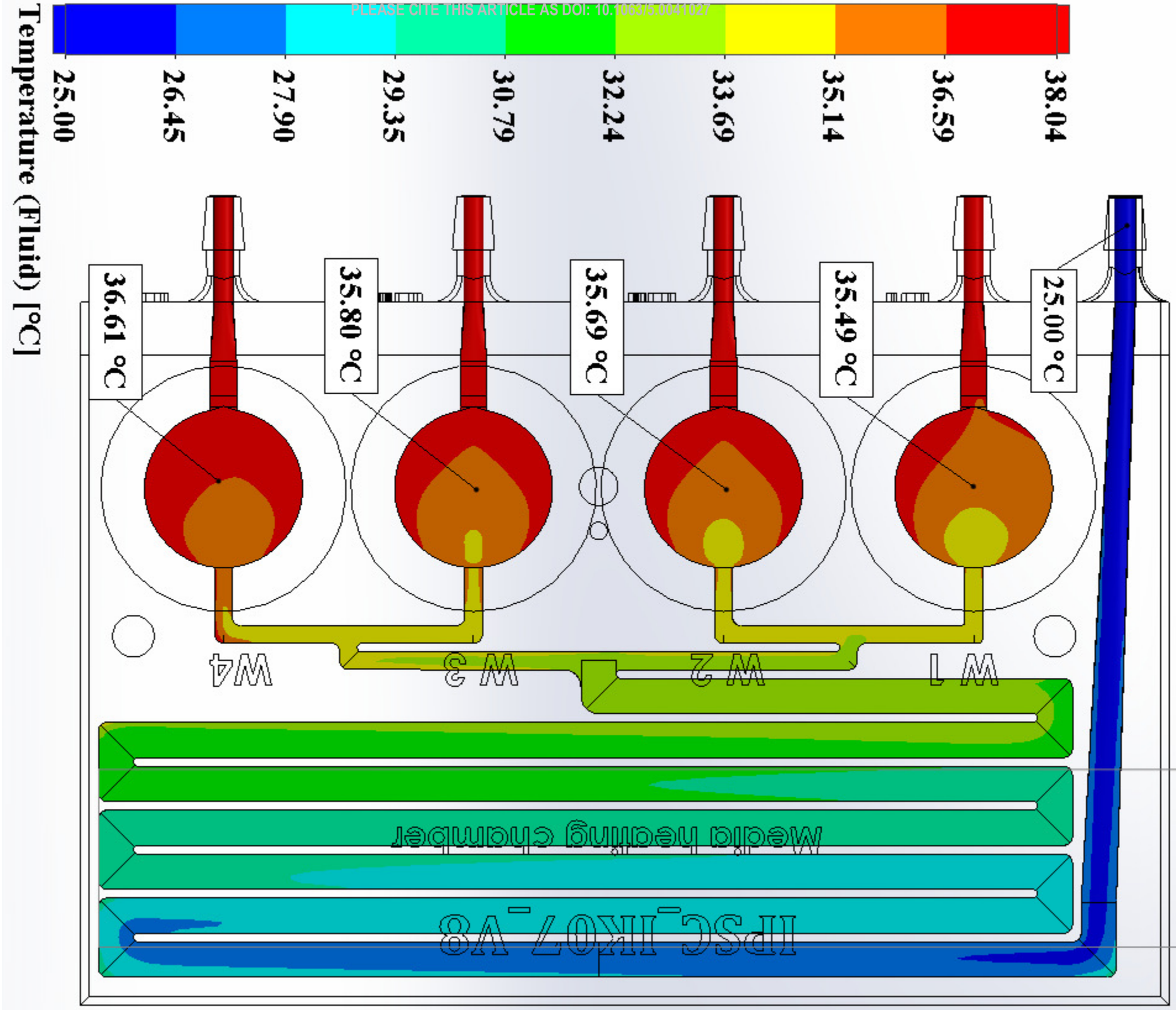

AIP Publishing

Biomicrofluidics

ACCEPTED MANUSCRIPT

PLEASE CITE THIS ARTICLE AS DOI: 10.1063/5.0041027

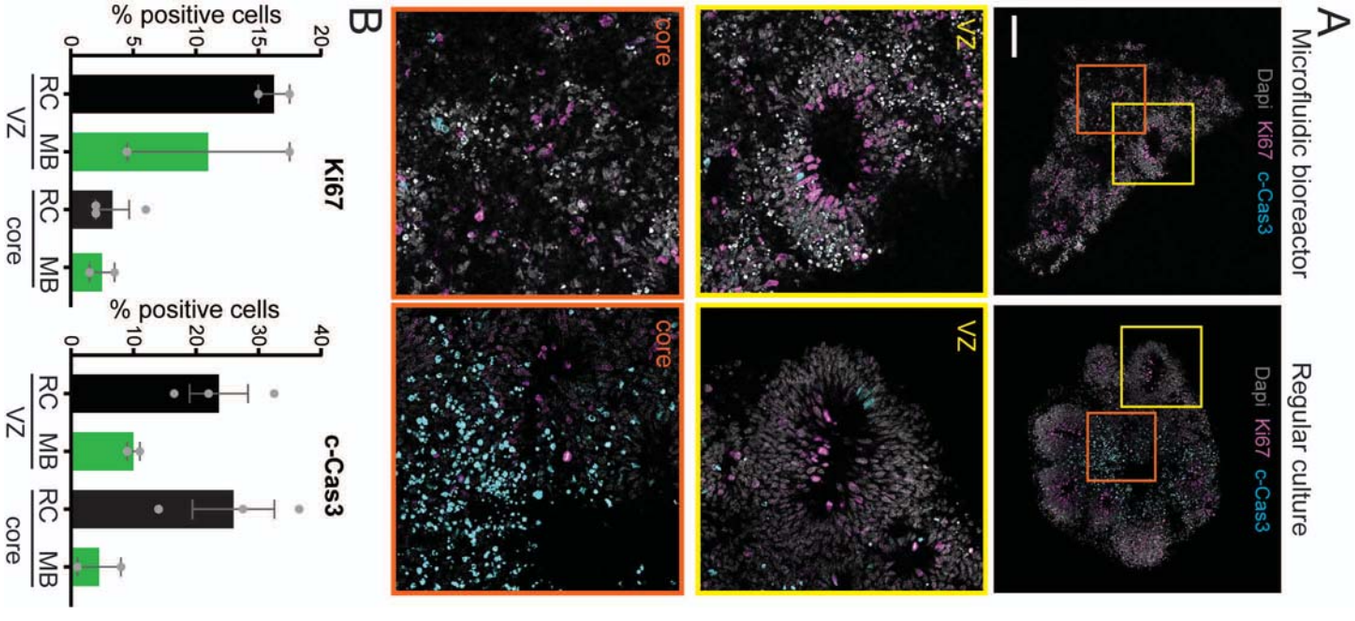

AIP Publishing

Biomicrofluidics

ACCEPTED MANUSCRIPT

This is the author's peer reviewed, accepted manuscript. However, the online version of record will be different from this version once it has been copyedited and typeset.
PLEASE CITE THIS ARTICLE AS DOI: 10.1063/5.0041027

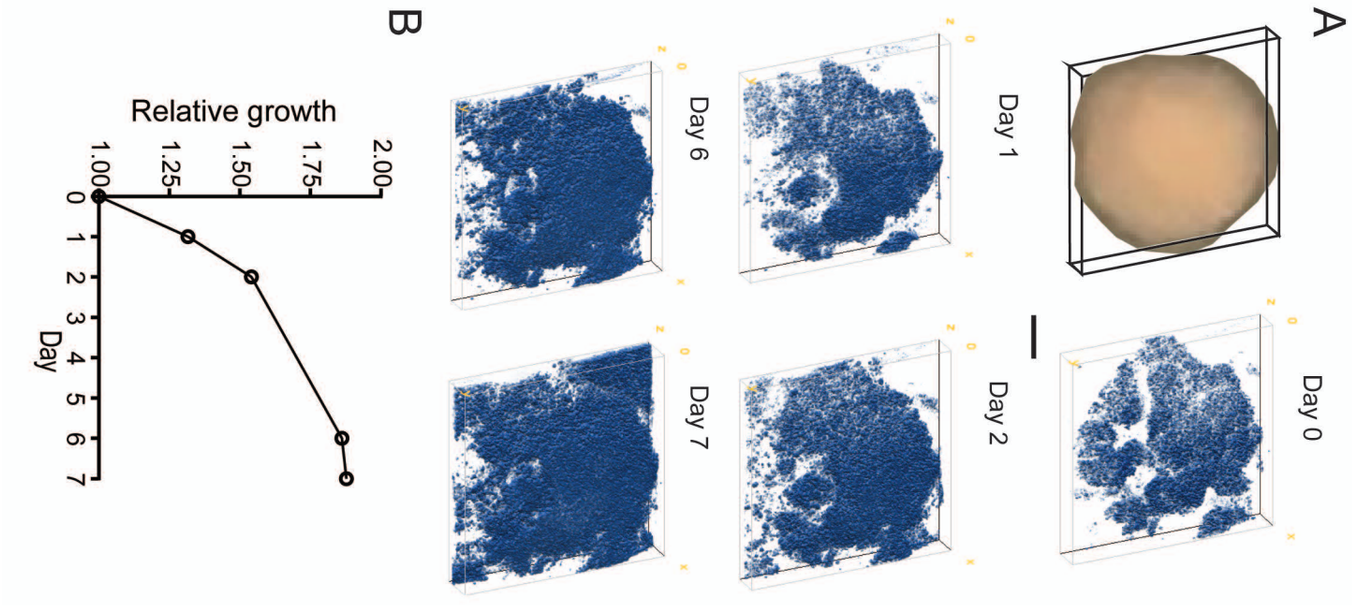

AIP Publishing

Biomicrofluidics

ACCEPTED MANUSCRIPT

This is the author's peer reviewed, accepted manuscript. However, the online version of record will be different from this version once it has been copyedited and typeset.
PLEASE CITE THIS ARTICLE AS DOI: 10.1063/5.0041027